Volume 16 | Number 27 | 21 July 2018 | Pages 4917–5056

Organic & Biomolecular Chemistry

rsc.li/obc

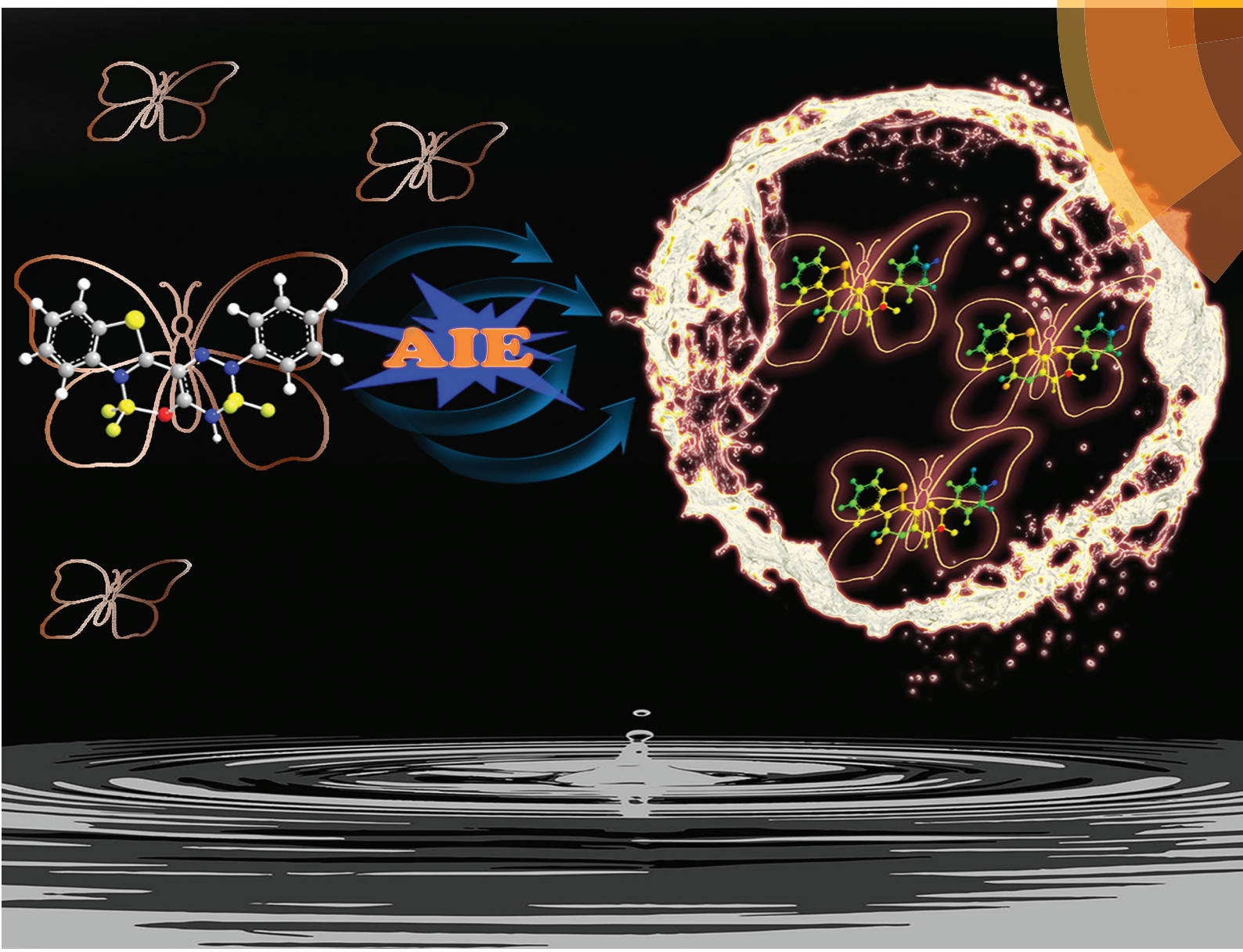

ISSN 1477-0520

ROYAL SOCIETY OF CHEMISTRY

PAPER
Shuwen Gong, Zhipeng Liu *et al.*
AIE-active boron complexes based on benzothiazole–hydrazone chelates

Organic & Biomolecular Chemistry

PAPER

View Article Online
View Journal | View Issue

Cite this: *Org. Biomol. Chem.*, 2018, **16**, 4977

AIE-active boron complexes based on benzothiazole–hydrazone chelates†

Wenzeng Duan,‡[a] Qingsong Liu,‡[a] Yanmin Huo,[a] Jichun Cui,[a] Shuwen Gong*[a] and Zhipeng Liu *[b]

Received 30th March 2018,
Accepted 4th May 2018

DOI: 10.1039/c8ob00755a

rsc.li/obc

A new family of aggregation-induced emission (AIE)-active monoboron and bisboron complexes based on benzothiazole–hydrazone chelates was synthesized. These complexes showed very weak fluorescence in fluid solution due to active intramolecular rotation and were emissive in high-viscosity solvents or in the aggregation state. Single crystal X-ray diffraction analyses and theoretical calculations were carried out to explain AIE behavior. The large Stokes shifts (3590–7400 cm^{-1}) and relatively highly efficient solid-state emission make these complexes valuable AIE luminophores for further potential applications.

Introduction

The design and synthesis of luminescent boron complexes has attracted substantial interest because of their extensive use in diverse areas.[1–3] Various luminescent boron complexes including three- and four-coordinate boron complexes have been studied.[4–6] Among them, those with efficient luminescence in solution and/or in the solid state are of particular interest for their practical applications in fluorescent sensing and imaging, and optoelectronic devices.[7–10] However, many luminescent boron complexes, especially the famous boron dipyrromethene (BODIPY) dyes, show small Stokes shift and rarely show fluorescence in the solid state.[1,4] Therefore, the development of new BODIPY dyes with high solid-state emission is being actively investigated.

Aggregation-induced emission (AIE) is an efficient strategy to create solid-state emissive luminophores.[11] In recent years, AIE has also been successfully employed for the development of solid-state emissive boron complexes.[12–15] Moreover, AIE-active boron complexes, especially those with low symmetry structures, exhibit both a large Stokes shift and intense fluorescence in the solid state.[16–19] On the other hand, in recent years, binuclear boron complexes have also gained much attention due to their interesting properties such as long-wavelength absorption and emission, nonlinear optical properties, and solid-state emission.[20–25] However, the study of the AIE properties of boron complexes, especially for binuclear boron complexes, is still limited. It is expected that the better understanding of the AIE phenomenon of both monoboron complexes and binuclear boron complexes is instructive to achieve novel AIE-active boron complexes and expand the scope of various applications.

Heterocyclic based hydrazones are useful building blocks for the generation of new luminescent complexes.[26] Indeed, some borondifluoride (BF_2)–hydrazone complexes (BODIHYs) display a large Stokes shift, AIE and intense emission in the solid state (Fig. 1).[16] These reports suggest that the BF_2–hydrazone complexes could be an important AIE–luminophore system. Nonetheless, the systems that efficiently emit in the solid-state are still under development, and the better under-

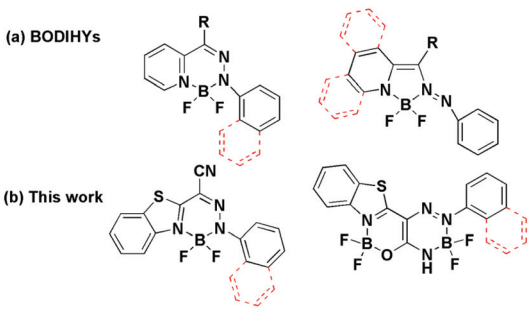

Fig. 1 Chemical structures of hydrazine-based boron complexes (BODIHYs) and compounds **6–7**.[31]

[a]*Institute of Functional Organic Molecules and Materials, School of Chemistry and Chemical Engineering, Liaocheng University, No.1 Hunan Road, Liaocheng, 252000, People's Republic of China. E-mail: gongshw@lcu.edu.cn*
[b]*Key Laboratory of Flexible Electronics (KLOFE) & Institute of Advanced Materials (IAM), Jiangsu National Synergetic Innovation Center for Advanced Materials (SICAM), Nanjing Tech University (Nanjing Tech), 30 South Puzhu Road, Nanjing, 211816, P.R. China. E-mail: iamzpliu@njtech.edu.cn*

†Electronic supplementary information (ESI) available: ^1H, ^{13}C NMR and luminescence spectra of compounds **6a**, **6b**, **7a** and **7b**. CCDC 1470184, 1470187, 1470185 and 1470189. For ESI and crystallographic data in CIF or other electronic format see DOI: 10.1039/c8ob00755a

‡Both authors contribute equally to this work.

standing of the AIE phenomenon in these complexes is still required. In the course of our studies on the development of aggregation-state emissive boron complexes, we are interested in the development of AIE-active boron complexes.[27–30] Herein, we report the synthesis and photoproperties of a new series of mono- and binuclear boron complexes (**6** and **7**, Fig. 1) based on benzothiazole–hydrazone chelates, which display a large Stokes shift and AIE.

Results and discussion

Synthesis of compounds 6–7

Compounds **6** and **7** were synthesized *via* a three-step procedure. The reaction of 2-(benzothiazol-2-yl)acetonitrile with diazonium salt gave the benzothiazole–hydrazone ligands **4**. We envisioned that the benzothiazole–hydrazone ligands **4** might be applied in the reaction with boron trifluoride diethyl ether as well due to their structural similarity with quinoline–hydrazone reported by Aprahamian *et al.* (Fig. 1a).[12,16] We anticipated that the six-membered compounds **6** and the five-membered compounds **8** would be formed *via* a similar process.[31] However, after the treatment of compounds **4** with boron trifluoride diethyl ether in dichloromethane in the presence of NEt_3, except for monoboron complexes **6**, none of the expected five-membered compounds **8** were obtained. We further explored the reaction in toluene under reflux conditions. Interestingly, besides the monoboron complexes **6**, unexpected bisboron complexes **7** were also obtained. The formation of these bisboron complexes is likely due to the hydrolysis of the nitrile group during the reaction to give the intermediate **5** (Scheme 1).[32] These complexes were characterized by ^1H, ^{13}C NMR and ESI-MS spectroscopy and single crystal X-ray diffraction.

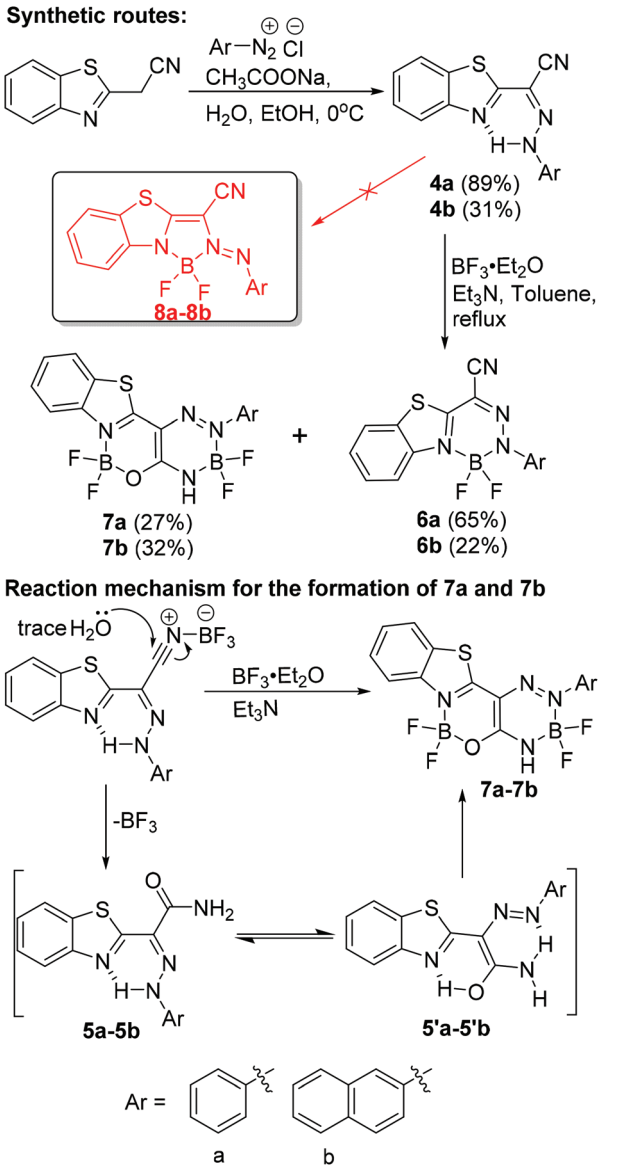

Scheme 1 Synthetic routes and reaction mechanism for compounds **6–7**.

Photophysical properties

The photophysical properties of compounds **6a**, **6b**, **7a** and **7b** were measured in different solvents and in the solid state. Full details can be found in Fig. 2 and Table 1. In tetrahydrofuran (THF), **6a** showed absorption maxima (λ_{abs}) at 434 nm (ε = 47 000 M^{-1} cm^{-1}), while **6b** showed λ_{abs} at 398 nm (ε = 57 000 M^{-1} cm^{-1}). This blue-shift of the absorption band should be attributed to the inhibited molecular conjugation between naphthyl with the BF_2 centre induced by the steric hindrance effect of the bulky naphthyl substituent in compound **6b**. Moreover, compounds **7a** and **7b** showed absorption bands with λ_{abs} at 420 nm (ε = 76 000 M^{-1} cm^{-1}) and 394 nm (ε = 41 000 M^{-1} cm^{-1}), respectively (Fig. 2, Fig. S1† and Table 1). The slightly blue-shifted λ_{abs} of **7a** and **7b** suggests that the introducing of another boron atom probably has less electronic effect on the ground states compared with the monoboron complexes **6a** and **6b**.

Compounds **6a**, **6b**, **7a** and **7b** showed weak emission (Φ_f < 0.01) in THF. Due to the greater electron delocalization ability in the excited states and a larger π-conjugation plane of the naphthyl substituent, compounds **6b** and **7b** showed red-shifted emission maxima (F_{max}, 524 and 556 nm for **6b** and **7b**, respectively) compared to compounds **6a** and **7a** (F_{max}, 514 and 506 nm for **6a** and **7a**, respectively).[33] Moreover, the red-shifted emission of **7b** compared to **6b** may also indicate that the naphthyl substituent leads to the better conjugation of bisboron complexes than the monomer ones in the excited states (Fig. 2 and Table 1).

The solvent effect on the absorption spectra of **6a**, **6b**, **7a** and **7b** was examined (Fig. S1†). In different solvents, **6a**, **6b**, **7a** and **7b** showed similar absorption peaks, suggesting the absorption spectra were hardly affected by solvent polarity. As shown in Fig. 3, **6a**, **6b**, **7a** and **7b** exhibited very weak fluorescence in low-viscosity solvents (Φ_f < 0.01), whereas in high-viscosity solvents such as glycerol, the fluorescence intensity of these compounds showed significant enhancement, with Φ_f of

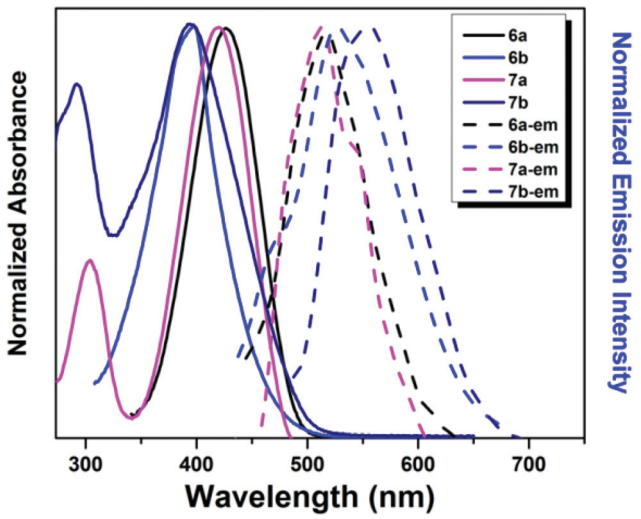

Fig. 2 Normalized absorption and luminescence spectra of compounds **6a**, **6b**, **7a** and **7b** (10^{-5} M) in THF.

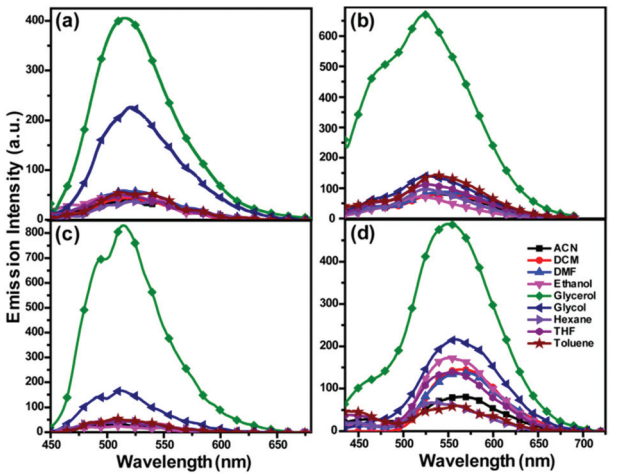

Fig. 3 Normalized luminescence spectra of compounds **6a** (a), **6b** (b), **7a** (c) and **7b** (d) in various solvents (10^{-5} M) such as hexane, toluene, dichloromethane (DCM), tetrahydrofuran (THF), acetonitrile (ACN), dimethylformamide (DMF), ethanol, ethylene glycol (glycol) and glycerol, respectively.

0.05 for **6a**, 0.06 for **6b**, 0.02 for **7a**, and 0.01 for **7b**, respectively (Table 1). This result suggests that the non-radiative relaxation of the excited luminophore is impeded by the higher solvent viscosity *via* restricted intramolecular rotation of aromatic rings, which is typical AIE behavior.[11,27–30] Additionally, the Stokes shifts of **6a**, **6b**, **7a** and **7b** are in the range 3590–7400 cm^{-1} (Table 1), which are larger than those of fluorescent boron complexes such as BODIPY (400–600 cm^{-1}) and benzothiazole-enamide-based BF_2 complexes (2190–4070 cm^{-1}).[29]

The AIE properties of **6a**, **6b**, **7a** and **7b** were investigated in binary solvent systems of THF–water with different water fractions (Fig. 4, Fig. S2† and Table 1). The fluorescence intensities of **6a**, **6b** and **7a** were very weak in pure THF. When water was added to the THF solution, the fluorescence intensities of **6a**, **6b** and **7a** remained almost the same until the water fraction (f_w) reached 90%. In contrast, the fluorescence intensity of **7b** increased progressively with the increment of f_w, and reached the maximum at f_w of 90%. Importantly, the fluorescence intensities of **6a**, **6b**, **7a** and **7b** at f_w of 99% increased by 8-fold, 9-fold, 8-fold and 2-fold, respectively, than those at f_w of 0% (Fig. S2†). **6a**, **7a**, and **7b** showed red-shifted emission

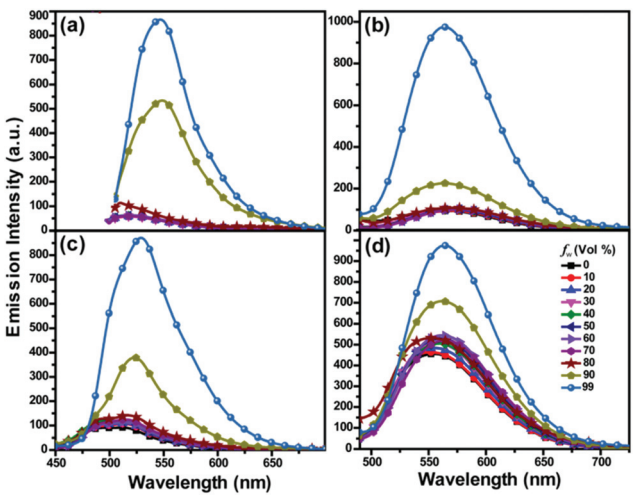

Fig. 4 Emission spectra of **6a** (a), **6b** (b), **7a** (c), and **7b** (d) in THF/water mixtures (10 μM) with varied volumetric fractions of water (f_w).

Table 1 Photophysical data of compounds **6** and **7** in solution and in the solid state

	In solution				In the solid state[f]				
Cpd	λ_{abs} (nm) ε (mol^{-1} cm^{-1})[a]	λ_{em} (nm) (Φ_f) solu.[a]	λ_{em} (nm) (Φ_f) aggr.[b,c]	λ_{em} (nm) (Φ_f) glycerol[b]	SS[d] (cm^{-1})	λ_{abs} (nm)	λ_{em} (nm)	Φ_f[e]	SS[d] (cm^{-1})
6a	434 (47 000)	514 (<0.01)	549 (<0.01)	516 (0.05)	3590	426	573	0.02	6020
6b	398 (57 000)	524 (<0.01)	564 (0.01)	524 (0.06)	6040	398	543	0.01	6710
7a	305 (33 000), 420 (76 000)	506 (<0.01)	523 (0.01)	514 (0.02)	4050	418	541	0.10	5440
7b	292 (35 000), 394 (41 000)	556 (<0.01)	562 (<0.01)	549 (0.01)	7400	394	560	0.01	7530

[a] Measured at a concentration of 10 μM in THF at 25 °C. [b] Determined using 4-methylamino-7-nitro-2,1,3-benzoxadiazole (Φ_f = 0.38 in acetonitrile) as reference.[34,35] [c] Measured at a concentration of 50 μM in THF/H_2O mixture with f_w of 90% at 25 °C. [d] Frequency units between the longest absorption band and the emission band. [e] Absolute quantum yield determined by calibrated integrating sphere systems. [f] Powder samples were used for the absolute quantum yield determination, absorption and emission spectra collection.

(35 nm, 17 nm and 6 nm) with the increase in f_w, suggesting a weak CT enhancement induced by aggregation. As mentioned above, aggregation by adding water to the THF solutions of **6** and **7** resulted in enhanced intensity and red-shifted emission. On the other hand, the AIE properties of **6**–**7** are mainly due to the aggregation formation that restricts free rotation of the aromatic ring.[11,27]

In the solid state, **6a**, **6b**, **7a** and **7b** showed λ_{abs} at 426 nm, 398 nm, 418 nm and 394 nm, respectively (Fig. 5 and Table 1). The emission bands of **6a**, **6b**, **7a** and **7b** are narrow and the F_{max} values are 573 nm, 543 nm, 541 nm and 560 nm, respectively (Fig. 5 and Table 1). Compared with the emission in solution, **6b** and **7b** showed a red-shifted emission of 19 and 4 nm, while **6a** and **7a** showed a larger emission red-shift of 59 and 35 nm, respectively. These results are in line with the aggregation-induced emission red-shifts in THF/water mixtures (Fig. 4). Importantly, **6a**, **6b**, **7a** and **7b** showed moderate emission with Φ_f of 0.02, 0.01, 0.10 and 0.01, respectively. This result suggests that the interactions of **6a**, **6b**, **7a** and **7b** should be weak in the solid state, which is in agreement with the results obtained from X-ray crystal structure analysis. Moreover, **6**–**7** showed larger Stokes shifts in the solid state (5440–7530 cm^{-1}) than in solution. The narrow emission band and a large Stokes shift should be another reason for the intense emission of **6a**, **6b**, **7a** and **7b** in the solid state.

X-Ray crystal structure analysis

Single crystal X-ray crystallographic analysis was performed to better understand the aggregation mechanism and solid-state emission properties of each compound. The ORTEP drawings and the packing structures of **6**–**7** are shown in Fig. 6 and Fig. S3.† **6**–**7** belong to the same cell setting (monoclinic) and different space groups ($P2(1)/c$ for **6a**, **6b** and **7a** and $P2(1)/n$ for **7b**). All the boron atoms in the compounds **6**–**7** adopt a tetrahedral geometry to form *N*^*N*-chelate six-membered rings and *N*^*O*-chelate six-membered rings, which contribute to the construction of the three-ring-fused and four-ring-fused

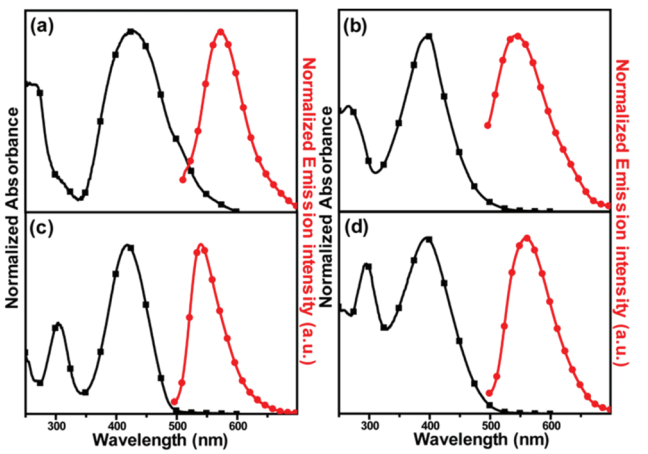

Fig. 5 The solid-state absorption and emission spectra of compounds **6a** (a), **6b** (b), **7a** (c), and **7b** (d).

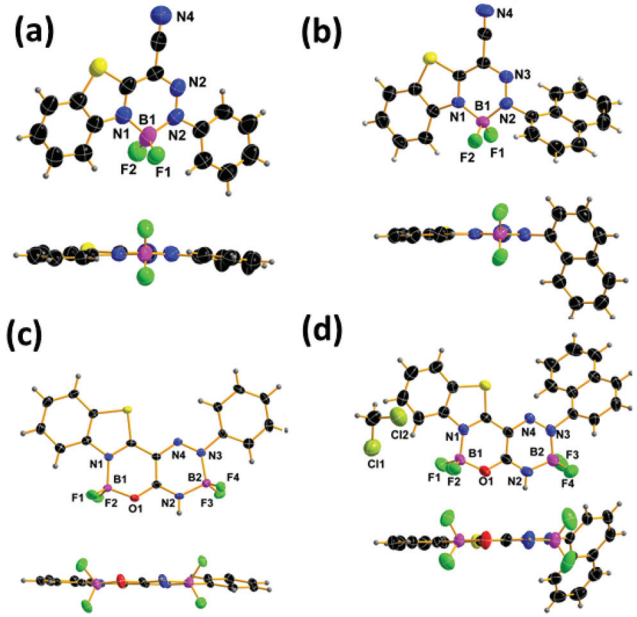

Fig. 6 Crystal structures of **6a** (a), **6b** (b), **7a** (c) and **7b** (d) (50% probability for thermal ellipsoids).

π-conjugated skeletons. **6a** and **7a** adopt tetrahedral conformations and the phenyl rings are almost coplanar, while the naphthyl rings in **6b** and **7b** are not coplanar, and the dihedral angles of *N*^*N*-chelate six-membered rings and the plane of naphthyl rings are 66.76° for **6b** and 55.78° for **7b**, respectively, indicating the larger steric effect of the naphthyl than the phenyl ring.

Clearly, weak intermolecular π–π interactions were observed in **6a**, **7a** and **7b** with the distance 3.688 Å in **6a**, 2.769 Å in **7a**, and 3.772 Å in **7b** (Fig. S3†). Molecules in adjacent chains adopt a typical mode of head-to-head or head-to-tail packing arrangements. In essence, multiple short intermolecular contacts exist in the crystals: F1···H3–C3 (2.67 Å, 12.47°), F2···H14–C14 (2.42 Å, 177.68°), and N4···H17–C17 (2.62 Å, 142.40°) interactions in **6a**, F1···H3–C3 (2.38 Å, 142.94°) and F1···H11–C11 (2.48 Å, 170.22°), F2···H12–C12 (3.13 Å, 110.54°), N4–C7 (3.20 Å) and N4–C8 (3.22 Å) interactions in **6b**, F1···H4–C4 (2.60 Å, 144.16°), F2···H18–N2 (2.67 Å, 118.03°), O1···H3–C3 (2.59 Å, 150.57°) and F4···H18–N2 (2.39 Å, 132.95°) interactions in **7a**, and F2···H41–N6 (2.24 Å, 144.32°), F3···H41–N6 (2.67 Å, 116.04°), F5···H40–N2 (2.45 Å, 147.01°), F8···H40–N2 (2.62 Å, 120.76°) and S1–S2 (3.55 Å) interactions in **7b**. These weak intermolecular interactions could help to fix the molecular conformations of **6**–**7** in the solid state, thus inhibiting the internal rotations and blocking their non-radiative relaxation. The results agree with the optical properties that **6**–**7** show moderate emissions in the solid state.

Theoretical calculations

Time-dependent density functional theory (TD-DFT) calculations were also performed to give an in-depth insight into the photophysical properties of **6**–**7**.[36] The calculations were

performed in the gas phase with the crystal structures used as a model structure with geometry optimization. The energy level alignment and the pictorial drawings of HOMOs and LUMOs of **6–7** are shown in Fig. 7 and Table S1.†

The calculated excited states have excitation energies of 3.01 eV (411 nm, $f = 0.6862$) for **6a**, 3.50 eV (355 nm, $f = 0.4950$) for **6b**, 3.06 eV (405 nm, $f = 0.8369$) for **7a** and 3.51 eV (354 nm, $f = 0.4844$) for **7b**, respectively. The results are almost in agreement with the experimental results (Table 1). As for **6a** and **7a**, the maximum absorption bands can be assigned to the transitions from the HOMO to the LUMO. However, for **6b** and **7b**, the oscillator strengths of the transitions from the HOMO to the LUMO are lower (0.1922 for **6b** and 0.2125 for **7b**), indicating that their maximum absorption bands are mainly contributed by the transition from HOMO−1 to the LUMO. In **6a** and **7a**, the HOMOs and LUMOs are delocalized across the whole molecular backbone, owing to the conjugated molecular geometry. The (HOMO−1)s of **6b** and **7b** are localized on the whole molecular backbone, while their LUMOs are localized mainly on the benzothiazole group and the six-membered ring containing a boron atom. For all the compounds, due to the high electron withdrawing ability of the BF_2 centre, the electron density in LUMOs has distribution in the context of the BF_2 group, which may result in the low LUMO level.

Compared with **7a**, the energy of the HOMO of **6a** is higher, which results in a decrement in the HOMO–LUMO gap, leading to a red shift of the absorption of **6a** relative to that of **7a**. The LUMOs of **6a** and **7a** are slightly lower in energy than those of **6b** and **7b**, which is due to the incorporation of the naphthyl group. The incorporation of the naphthyl group in **6b** and **7b** also greatly decreased the HOMO energy level by 0.45 eV and 0.42 eV. Thus, these results indicate that the aromatic unit in **6–7** could tune the main absorption bands efficiently,[37] and that the theoretical calculations can predict the extent of the shift of the absorption bands (Fig. S4†).

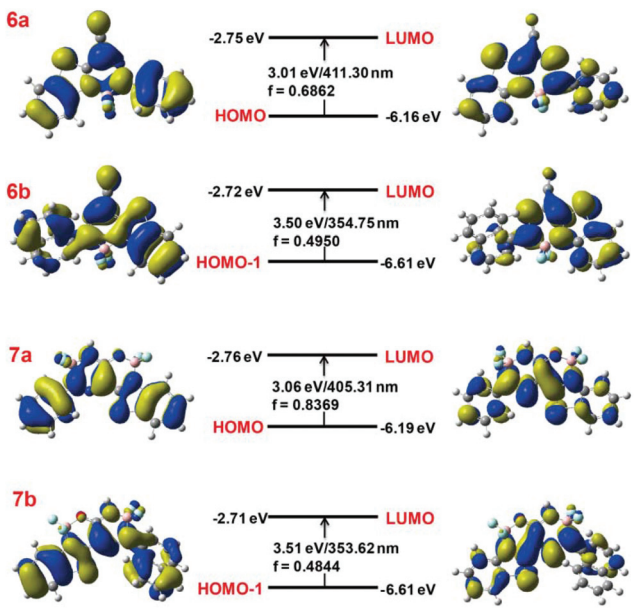

Fig. 7 Molecular orbital amplitude plots and energy levels of the HOMOs and LUMOs of compounds **6–7**, calculated using the B3LYP/6-31G(d,p) basis set with the G03 software package.

Conclusions

In summary, a new family of benzothiazole–hydrazone-based boron complexes (**6** and **7**) were developed by the reaction of benzothiazole–hydrazone-based desymmetrized *N*,*N*-bidentate ligands with boron trifluoride etherate. Compounds **6** and **7** exhibited AIE characteristics and fluorescence efficiently in the aggregate state. The four complexes showed weak emission in low-viscosity organic solvents because of the intramolecular rotation that induces the non-radiative process. Their emission can be dramatically enhanced by the increase in solvent viscosity or by molecular aggregation in the solid state. X-ray crystallographic analysis showed that weak intermolecular interactions such as F···H–C and O···H–C fix the molecular conformations of **6** and **7**, which are responsible for the intense fluorescence in the solid state. The theoretical calculation results indicate that the aromatic unit in **6–7** can tune the main absorption bands. Moreover, the large Stokes shifts and the strong solid-state emission of **6** and **7** render them valuable AIE luminophores for potential application in the fields of biological imaging and materials science.

Experimental

General information

All reactions and manipulations of air-sensitive compounds were carried out under an argon atmosphere using Schlenk techniques and/or vacuum line techniques. Solvents were dried prior to use by common methods in organometallic chemistry. Chemicals were commercially obtained and used as received. ^{1}H, ^{11}B and ^{13}C NMR spectra were recorded using a Varian Mercury-plus 400 M spectrometer instrument. Chemical shifts were reported in ppm relative to $Si(CH_3)_4$ (^{1}H, ^{13}C), and coupling constants (J) are given in Hz. Mass spectra were obtained on an LCQ (ESI-MS, Thermo Finnigan) mass spectrometer. Thin layer chromatography (TLC) was performed on plates coated with thick silica gel GF254 (Qingdao Haiyang Chemical Co., Ltd). Column chromatography was performed using silica gel (200 mesh, Qingdao Haiyang Chemical Co., Ltd).

Synthesis

Synthesis of 4a and 4b. Aniline or naphthylamine (1.0 equiv., 10 mmol) and 4 mL of ice cold water were dissolved in a mixture of 6 mL HCl, and stirred at 0 °C for 30 min. A cold solution (3 mL water) of sodium nitrite (1.0 equiv., 0.69 g, 10 mmol) was then added drop-wise to the aniline solution at 0–5 °C. The resulting light yellow solution was continuously

stirred for 1.5 hours at −5 °C. The obtained diazonium salt solution was then added drop-wise to a suspension of 2-benzothiazoleacetonitrile (0.8 equiv., 1.39 g, 8 mmol) and sodium acetate (3.2 equiv., 2.62 g, 32 mmol) in a cold mixture of ethanol (60 mL) and water (30 mL). The resulting reaction mixture was stirred at room temperature overnight. The crude was obtained by filtration and recrystallization.

Compound 4a. Yield: 89%. ^{1}H NMR (400 MHz, $CDCl_3$) δ/ppm = 14.35 (s, 1H), 8.05 (d, J = 8.2 Hz, 1H), 7.95 (d, J = 8.0 Hz, 1H), 7.58 (t, J = 7.7 Hz, 1H), 7.49 (t, J = 7.6 Hz, 1H), 7.46–7.37 (m, 4H), 7.18 (t, J = 6.4 Hz, 1H); ^{13}C NMR (100 MHz, $CDCl_3$) δ/ppm = 160.1, 152.8, 141.7, 133.2, 129.8, 127.4, 126.8, 125.3, 123.0, 122.1, 116.9, 115.8; ESI-MS: calcd: $[M - H]^-$ = 277.3, found: $[M - H]^-$ = 277.1.

Compound 4b. Yield: 31%. ^{1}H NMR (400 MHz, $CDCl_3$) δ/ppm = 15.18 (s, 1H), 8.22–8.06 (m, 2H), 7.98 (d, J = 7.6 Hz, 1H), 7.90 (d, J = 7.5 Hz, 2H), 7.64 (dd, J = 18.3, 7.7 Hz, 3H), 7.54 (dt, J = 15.0, 7.5 Hz, 3H); ^{13}C NMR (100 MHz, $CDCl_3$) δ/ppm = 160.3, 152.7, 136.9, 134.3, 133.4, 129.1, 127.5, 126.9, 126.5, 125.5, 123.1, 122.9, 122.2, 119.7, 116.8, 111.6; ESI-MS: calcd: $[M - H]^-$ = 327.4, found: $[M - H]^-$ = 327.2.

Synthesis of 6a, 6b, 7a and 7b. Compound **4a** or **4b** (1 equiv.) was dissolved in dry toluene. Then DBU (3.0 equiv.) was added to the solution. After being stirred for 10 min at room temperature, $BF_3{\cdot}OEt_2$ (5.0 equiv.) was slowly added to the mixture *via* a syringe. The resulting mixture was heated to reflux for 2 h. After cooling to room temperature, the solution was extracted with dichloromethane. The organic layer was washed with water and brine, and dried over anhydrous magnesium sulfate. Column chromatography of the residue on silica gel gave the desired product.

Compound 6a. Yield: 65%, (petroleum ether : dichloromethane = 1 : 3, R_f = 0.6). ^{1}H NMR (400 MHz, $CDCl_3$) δ/ppm = 8.31 (d, J = 8.6 Hz, 1H), 7.98 (d, J = 7.9 Hz, 1H), 7.85 (d, J = 8.1 Hz, 2H), 7.74 (t, J = 7.8 Hz, 1H), 7.65 (t, J = 7.8 Hz, 1H), 7.47 (t, J = 7.9 Hz, 2H), 7.35 (t, J = 7.4 Hz, 1H); ^{13}C NMR (100 MHz, $CDCl_3$) δ/ppm = 157.9, 144.6, 142.8, 129.4, 128.2, 127.9, 122.8, 121.4, 120.2, 114.8; ^{11}B NMR (128 MHz, $CDCl_3$) δ/ppm = 2.07 (s), 1.16 (d, J = 31.7 Hz), 0.79 (s); HRMS (ESI): calcd, $[M + H]^+$ = 327.0685, found: $[M + H]^+$ = 327.0695.

Compound 6b. Yield: 22%, (DCM, R_f = 0.6).^{1}H NMR (400 MHz, $CDCl_3$) δ/ppm = 8.27 (d, J = 8.3 Hz, 1H), 8.02 (d, J = 7.9 Hz, 1H), 7.99–7.90 (m, 2H), 7.80–7.62 (m, 4H), 7.61–7.49 (m, 3H); ^{13}C NMR (100 MHz, $CDCl_3$) δ/ppm = 158.2, 142.9, 140.0, 134.8, 130.1, 130.1, 129.4, 128.4, 127.3, 126.7, 125.1, 123.9, 123.1, 122.8, 120.3, 114.6; ^{11}B NMR (128 MHz, $CDCl_3$) δ/ppm = 0.87 (s), 0.65 (s), 0.42 (s); HRMS (ESI): calcd, $[M + H]^+$ = 377.0842, found: $[M + H]^+$ = 377.0844, calcd, $[M + Na]^+$ = 399.0661, found: $[M + Na]^+$ = 399.0670.

Compound 7a. Yield: 27%, (petroleum ether : DCM = 1 : 3, R_f = 0.2). ^{1}H NMR (400 MHz, $CDCl_3$) δ/ppm = 8.18 (d, J = 8.4 Hz, 1H), 7.90 (d, J = 8.1 Hz, 1H), 7.85 (d, J = 8.1 Hz, 2H), 7.68 (t, J = 7.9 Hz, 1H), 7.58 (t, J = 7.6 Hz, 1H), 7.48 (t, J = 7.6 Hz, 2H), 7.40 (d, J = 7.3 Hz, 1H); ^{13}C NMR (100 MHz, $CDCl_3$) δ/ppm = 129.4, 129.1, 128.8, 127.5, 122.4, 121.5, 119.5; ^{11}B NMR (128 MHz, $CDCl_3$) δ/ppm = 0.66 (s), 0.32 (d, J = 29.5 Hz), 0.26–0.20 (m). HRMS (ESI): calcd, $[M - F]^+$ = 373.0714, found: $[M - F]^+$ = 373.0746; calcd, $[M + Na]^+$ = 415.0595, found: $[M + Na]^+$ = 415.0623.

Compound 7b. Yield: 32%, (DCM, R_f = 0.2). ^{1}H NMR (400 MHz, $CDCl_3$) δ/ppm = 8.19 (d, J = 8.3 Hz, 1H), 8.00–7.91 (m, 2H), 7.85–7.77 (m, 2H), 7.73 (d, J = 7.4 Hz, 1H), 7.67 (t, J = 7.9 Hz, 1H), 7.6–7.51 (m, 4H); ^{13}C NMR (100 MHz, $CDCl_3$) δ/ppm = 156.2, 143.0, 140.2, 134.7, 129.8, 129.5, 129.0, 128.4, 127.5, 126.6, 125.1, 123.4, 122.7, 122.4, 119.4; ^{11}B NMR (128 MHz, $CDCl_3$) δ/ppm = 0.28 (s), 0.07 (s), −0.14 (s). HRMS (ESI): calcd, $[M + Na]^+$ = 465.0752, found: $[M + Na]^+$ = 465.0738.

Spectroscopic measurements

UV-vis absorption spectra were recorded on a Shimadzu UV-3600 spectrometer with a resolution of 1.0 nm. A solution of the sample (*ca.* 1×10^{-5} M) in a 1 cm^2 quartz cell was used for the measurement. Fluorescence spectra were recorded on a Hitachi F-7000 spectrometer under the following conditions: excitation wavelength = 405 nm (**6a**), 400 nm (**6b**), 432 nm (**7a**) and 395 nm (**7b**), an excitation slit width of 15 nm and a PMT voltage of 775 V for **6a**, **7a** and **7b**, an emission slit width of 10 nm and a PMT voltage of 775 V for **6b**. Powder samples of **6a**, **6b**, **7a** and **7b** were used for the absorption and emission spectra recording. The fluorescence lifetimes and the absolute quantum yields (Φ_f) of the powder samples were determined with a Horiba JobinYvon Fluorolog-3 spectrofluorimeter. Fluorescence quantum yields of **6a**, **6b**, **7a** and **7b** in solution were determined using 4-methylamino-7-nitro-2,1,3-benzoxadiazole (Φ_f = 0.38) in acetonitrile as the reference.[38]

X-ray structure determination

X-ray diffraction data were collected at 298 K on a Gemini A single crystal CCD X-ray diffractometer with MoK_α radiation (l = 0.71073 Å) and graphite monochromator. The structure was solved by direct methods (SHELX-97)[39] and refined by the full-matrix least-squares on F^2 (SHELX-97). All the non-hydrogen atoms were refined anisotropically and all the hydrogen atoms were placed using AFIX instructions.

Compound 6a. $C_{15}H_9BF_2N_4S$; M = 326.13, monoclinic, space group $P2(1)/c1$, a = 11.0689(6) Å, b = 10.5398(5) Å, c = 25.7733 (15) Å, α = 90.00°, β = 109.097°, γ = 90.00°, V = 2841.3 (3) Å^3, T = 293(2) K, Z = 8, the final R = 0.0834 and wR = 0.2111 for 5092 observed reflections ($I > 2\sigma(I)$). GOF = 1.038. CCDC 1470184.†

Compound 6b. $C_{19}H_{11}BF_2N_4S$; M = 376.19, monoclinic, a = 13.7279(18) Å, b = 8.6809(13) Å, c = 14.7591(17) Å, α = 90.00°, β = 105.207°, γ = 90.00°, V = 1697.3(4) Å^3, T = 293(2) K, space group $P2(1)/c1$, Z = 4, the final R = 0.0524 and wR = 0.0979 for 3000 observed reflections ($I > 2\sigma(I)$). GOF = 1.046. CCDC 1470187.†

Compound 7a. $C_{31}H_{22}B_4F_8Cl_2N_8O_2S_2$; M = 868.83, monoclinic, a = 9.0994(6) Å, b = 17.1180(10) Å, c = 11.3594(9) Å, α = 90.00°, β = 98.095°, γ = 90.00°, V = 1751.7(2) Å^3, T = 293(2) K, space group $P2(1)/c$, Z = 2, the final R = 0.0831 and wR = 0.2370 for 3135 observed reflections ($I > 2\sigma(I)$). GOF = 1.082. CCDC 1470185.†

Compound 7b. $C_{39}H_{26}B_4F_8Cl_2N_8O_2S_2$; M = 968.94, monoclinic, a = 10.6491(7) Å, b = 22.7467(13) Å, c = 17.0946 (10) Å, α = 90.00°, β = 104.248°, γ = 90.00°, V = 4013.5(4) Å^3, T = 293(2) K, space group $P2(1)/n$, Z = 4, the final R = 0.0678 and wR = 0.1705 for 7079 observed reflections ($I > 2\sigma(I)$). GOF = 1.035. CCDC 1470189.†

Computational details

TD-DFT calculations were performed at the hybrid density functional theory level (B3LYP) with the 6-31G(d,p) basis set, using the Gaussian03 software package. The calculations were made in the gas phase.

Conflicts of interest

There are no conflicts to declare.

Acknowledgements

We thank the National Key R&D Program of China (2017YFA0207201), the Natural Science Foundation of China (21501085), the Natural Science Foundation of Shandong Province (ZR2017MB052, ZR2017MB060), the Key University Science Research Project of Jiangsu Province (17KJA150004) and the Liaocheng University Funds for Young Scientists (31805) for financial support.

Notes and references

1 H. Lu, J. Mack, Y. Yang and Z. Shen, *Chem. Soc. Rev.*, 2014, **43**, 4778.
2 F. Jäkle, *Chem. Rev.*, 2010, **110**, 3985.
3 K. Liu, R. A. Lalancette and F. Jäkle, *J. Am. Chem. Soc.*, 2017, **139**, 18170.
4 D. Frath, J. Massue, G. Ulrich and R. Ziessel, *Angew. Chem., Int. Ed.*, 2014, **53**, 2290.
5 Y. L. Rao, H. Amarne and S. Wang, *Coord. Chem. Rev.*, 2012, **256**, 759.
6 K. Tanaka and Y. Chujo, *NPG Asia Mater.*, 2015, **7**, e223.
7 D. Li, H. Zhang and Y. Wang, *Chem. Soc. Rev.*, 2013, **42**, 8416.
8 T. Kowada, H. Maeda and K. Kikuchi, *Chem. Soc. Rev.*, 2015, **44**, 4953.
9 C. T. Poon, D. Wu and V. W. Yam, *Angew. Chem., Int. Ed.*, 2016, **55**, 3647.
10 Z. Yu, Y. Wu, L. Xiao, J. Chen, Q. Liao, J. Yao, *et al.*, *J. Am. Chem. Soc.*, 2017, **139**, 6376.
11 J. Mei, N. L. Leung, R. T. Kwok, J. W. Lam and B. Z. Tang, *Chem. Rev.*, 2015, **115**, 11718.
12 H. Qian, M. E. Cousins, E. H. Horak, A. Wakefield, M. D. Liptak and I. Aprahamian, *Nat. Chem.*, 2017, **9**, 83.
13 R. Yoshii, A. Hirose, K. Tanaka and Y. Chujo, *J. Am. Chem. Soc.*, 2014, **136**, 18131.
14 M. Koch, K. Perumal, O. Blacque, J. A. Garg, R. Saiganesh, S. Kabilan, *et al.*, *Angew. Chem., Int. Ed.*, 2014, **53**, 6378.
15 Z. Zhao, Z. Chang, B. He, B. Chen, C. Deng, P. Lu, *et al.*, *Chem. – Eur. J.*, 2013, **19**, 11512.
16 Y. Yang, X. Su, C. N. Carroll and I. Aprahamian, *Chem. Sci.*, 2012, **3**, 610.
17 J. F. Araneda, W. E. Piers, B. Heyne, M. Parvez and R. McDonald, *Angew. Chem., Int. Ed.*, 2011, **50**, 12214.
18 D. Zhao, G. Li, D. Wu, X. Qin, P. Neuhaus, Y. Cheng, *et al.*, *Angew. Chem., Int. Ed.*, 2013, **52**, 13676.
19 R. Yoshii, A. Hirose, K. Tanaka and Y. Chujo, *Chem. – Eur. J.*, 2014, **20**, 8320.
20 Y. Kubota, K. Kasatani, T. Niwa, H. Sato, K. Funabiki and M. Matsui, *Chem. – Eur. J.*, 2016, **22**, 1816.
21 Y. Kubota, T. Niwa, J. Jin, K. Funabiki and M. Matsui, *Org. Lett.*, 2015, **17**, 3174.
22 D. Li, K. Wang, S. Huang, S. Qu, X. Liu, Q. Zhu, *et al.*, *J. Mater. Chem.*, 2011, **21**, 15298.
23 D. Li, Y. Yuan, H. Bi, D. Yao, X. Zhao, W. Tian, *et al.*, *Inorg. Chem.*, 2011, **50**, 4825.
24 J. Feng, B. Liang, D. Wang, L. Xue and X. Li, *Org. Lett.*, 2008, **10**, 4437.
25 G. M. Fischer, A. P. Ehlers, A. Zumbusch and E. Daltrozzo, *Angew. Chem., Int. Ed.*, 2007, **46**, 3750.
26 A. M. Stadler, F. Puntoriero, S. Campagna, N. Kyritsakas, R. Welter and J. M. Lehn, *Chem. – Eur. J.*, 2005, **11**, 3997.
27 X. Wang, Y. Wu, Q. Liu, Z. Li, H. Yan, C. Ji, *et al.*, *Chem. Commun.*, 2015, **51**, 784.
28 X. Wang, Q. Liu, H. Yan, Z. Liu, M. Yao, Q. Zhang, *et al.*, *Chem. Commun.*, 2015, **51**, 7497.
29 Q. Liu, X. Wang, H. Yan, Y. Wu, Z. Li, S. Gong, *et al.*, *J. Mater. Chem. C*, 2015, **3**, 2953.
30 F. Qi, J. Lin, X. Wang, P. Cui, H. Yan, S. Gong, *et al.*, *Dalton Trans.*, 2016, **45**, 7278.
31 Y. Yang, R. P. Hughes and I. Aprahamian, *J. Am. Chem. Soc.*, 2014, **136**, 13190.
32 K. T. Ashitha, V. P. Kumar, C. T. F. Salfeena and B. S. Sasidhar, *J. Org. Chem.*, 2018, **83**, 113.
33 J. Wan, C. J. Zheng, M. K. Fung, X. K. Liu, C. S. Lee and X. H. Zhang, *J. Mater. Chem.*, 2012, **22**, 4502.
34 F. Qian, C. Zhang, Y. Chang, W. He, X. Gao, P. Hu and Z. Guo, *J. Am. Chem. Soc.*, 2009, **131**, 1460.
35 S. Uchiyama, Y. Matsumura, A. P. de Silva and K. Iwai, *Anal. Chem.*, 2003, **75**, 5926.
36 M. J. Frisch, G. W. Trucks, H. B. Schlegel, G. E. Scuseria, M. A. Robb, J. R. Cheeseman, J. A. Montgomery Jr., T. Vreven, K. N. Kudin, J. C. Burant, J. M. Millam, S. S. Iyengar, J. Tomasi, V. Barone, B. Mennucci, M. Cossi, G. Scalmani, N. Rega, G. A. Petersson, H. Nakatsuji, M. Hada, M. Ehara, K. Toyota, R. Fukuda, J. Hasegawa, M. Ishida, T. Nakajima, Y. Honda, O. Kitao, H. Nakai, M. Klene, X. Li, J. E. Knox, H. P. Hratchian, J. B. Cross, V. Bakken, C. Adamo, J. Jaramillo, R. Gomperts, R. E. Stratmann, O. Yazyev, A. J. Austin, R. Cammi, C. Pomelli, J. W. Ochterski, P. Y. Ayala, K. Morokuma, G. A. Voth, P. Salvador, J. J. Dannenberg, V. G. Zakrzewski,

S. Dapprich, A. D. Daniels, M. C. Strain, O. Farkas, D. K. Malick, A. D. Rabuck, K. Raghavachari, J. B. Foresman, J. V. Ortiz, Q. Cui, A. G. Baboul, S. Clifford, J. Cioslowski, B. B. Stefanov, G. Liu, A. Liashenko, P. Piskorz, I. Komaromi, R. L. Martin, D. J. Fox, T. Keith, M. A. Al-Laham, C. Y. Peng, A. Nanayakkara, M. Challacombe, P. M. W. Gill, B. Johnson, W. Chen, M. W. Wong, C. Gonzalez and J. A. Pople, *Gaussian 03, Revision B.05*, Gaussian, Inc., Pittsburgh, PA, 2003.

37 H. J. Liu, X. J. Xu, H. N. Peng, X. M. Chang, X. W. Fu, Q. S. Li, S. W. Yin, G. J. Blanchard and Y. Fang, *Phys. Chem. Chem. Phys.*, 2016, **18**, 25210.

38 Y. P. Wu, Z. Y. Li, Q. S. Liu, X. Q. Wang, H. Yan, S. W. Gong, Z. P. Liu and W. J. He, *Org. Biomol. Chem.*, 2015, **13**, 5775.

39 G. M. Sheldrick, *SHELX-97, Program for the Refinement of Crystal Structures*, University of Göttingen, Göttingen, Germany, 1997.